RIP2 promotes FcγR-mediated reactive oxygen species production

Received for publication, December 18, 2018, and in revised form, May 2, 2019 Published, Papers in Press, May 21, 2019, DOI 10.1074/jbc.RA118.007218

Michael G. Shehat, Omar A. Cardona, George F. Aranjuez, Mollie W. Jewett, and Justine T. Tigno-Aranjuez[1]

From the Immunity and Pathogenesis Division, Burnett School of Biomedical Sciences, University of Central Florida College of Medicine, Orlando, Florida 32827

Edited by Luke O'Neill

Receptor-interacting protein 2 (RIP2) is a kinase that mediates signaling downstream of the bacterial peptidoglycan sensors NOD1 and NOD2. Genetic loss or pharmaceutical inhibition of RIP2 has been shown to be beneficial in multiple inflammatory disease models with the effects largely attributed to reducing proinflammatory signaling downstream of peptidoglycan recognition. However, given the widespread expression of this kinase and its reported interactions with numerous other proteins, it is possible that RIP2 may also function in roles outside of peptidoglycan sensing. In this work, we show that RIP2 undergoes tyrosine phosphorylation and activation in response to engagement of the Fc γ receptor (FcγR). Using bone marrow–derived macrophages from WT and RIP2-KO mice, we show that loss of RIP2 leads to deficient FcγR signaling and reactive oxygen species (ROS) production upon FcγR cross-linking without affecting cytokine secretion, phagocytosis, or nitrate/nitrite production. The FcγR-induced ROS response was still dependent on NOD2, as macrophages deficient in this receptor showed similar defects. Mechanistically, we found that different members of the Src family kinases (SFKs) can promote RIP2 tyrosine phosphorylation and activation. Altogether, our findings suggest that RIP2 is functionally important in pathways outside of bacterial peptidoglycan sensing and that involvement in such pathways may depend on the actions of SFKs. These findings will have important implications for future therapies designed to target this kinase.

The RIP2[2] kinase is a dual-specificity kinase that functions downstream of the pattern recognition receptors nuclear oligomerization domain proteins 1 (NOD1) and 2 (1–7). NOD1 and NOD2 recognize the bacterial peptidoglycan breakdown products γ-D-glutamyl-*meso*-diaminopimelic acid and *N*-acetylmuramyl-L-Ala-D-isoglutamine, respectively (8–10). The functional relevance of RIP2 within these peptidoglycan-sensing pathways has been demonstrated extensively by studies showing a crucial role for NOD2 and RIP2 in host defense against *Mycobacterium tuberculosis* (11), *Legionella pneumophila* (12), *Listeria monocytogenes* (3), *Salmonella enterica* (13), and *Chlamydophila pneumoniae* (14) to name a few.

RIP2 is not only more highly expressed in various tissues when compared with NOD1 or NOD2, but its expression is also less restricted (15). This, coupled with the fact that RIP2 also has numerous reported binding partners that are associated with a variety of signal transduction pathways, leads to an appealing scenario for the involvement of RIP2 in pathways outside of, or in conjunction with, NOD signaling. Previous reports studying this kinase implicated RIP2 as acting downstream of Toll-like receptors 2, 3, and 4, demonstrating defects in cytokine production as a result of lipopolysaccharide, lipoteichoic acid, peptidoglycan, and poly(I:C) stimulation (3). However, this was later disproven as the results were found to be a consequence of NOD agonists within the Toll-like receptor agonist preparations (5). Recent studies suggest that nerve growth factor acting through the p75 neurotrophin receptor ($p75^{NTR}$) can utilize RIP2 to promote survival in cerebellar granule neurons (16). This was demonstrated to occur by RIP2-mediated displacement of TNF receptor–associated factor 6 (TRAF6) from $p75^{NTR}$, leading to NF-κB activation and neuronal survival. Other studies have proposed a NOD1/2-independent, T-cell–intrinsic role for RIP2, with some groups suggesting that RIP2 prevents the generation of pathogenic IL-17A–producing T-cells (pTh17) (17) and others that RIP2 can interact with B cell leukemia 10 protein (Bcl10) and directly mediate its phosphorylation, leading to activation of NF-κB (18). However, multiple studies also exist demonstrating that

This work was supported, in part, by NHLBI, National Institutes of Health Grant R00HL122365 and University of Central Florida start-up funds (to J. T. T.-A.); NIAID, National Institutes of Health Grant R01AI099094 (to M. W. J.); and a Deborah and Mark Blackman-Global Lyme Alliance postdoctoral fellowship (to G. F. A.). The authors declare that they have no conflicts of interest with the contents of this article. The content is solely the responsibility of the authors and does not necessarily represent the official views of the National Institutes of Health.

This article contains Fig. S1 and Fig. S2.

[1] To whom correspondence should be addressed: Burnett School of Biomedical Sciences, University of Central Florida College of Medicine, 6900 Lake Nona Blvd., Orlando, FL 32827. Tel.: 407-266-7142; Fax: 407-266-7002; E-mail: justine.tigno-aranjuez@ucf.edu.

[2] The abbreviations used are: RIP2, receptor-interacting protein 2; ANOVA, analysis of variance; BMDM, bone marrow–derived macrophage; CCL, CC chemokine ligand; DMEM, Dulbecco's modified Eagle's medium; ERK, extracellular signal-regulated kinase; FBS, fetal bovine serum; FcγR, Fc γ receptor; FcRn, neonatal Fc receptor; HEK-293, human embryonic kidney 293 cells; GST, glutathione *S*-transferase; IFN-γ, interferon γ; IL, interleukin; IκBα, inhibitor of NF-κB, α; iNOS, inducible nitric-oxide synthase; IP, immunoprecipitation; ITAM, immunoreceptor tyrosine-based activation motif; IVK, *in vitro* kinase; JNK, Jun N-terminal kinase; KO, knockout; LAT, linker for activation of T-cells; MAPK, mitogen-activated protein kinase; MFI, mean fluorescence intensity; mIgG, mouse immunoglobulin G; NAC, *N*-acetyl-L-cysteine; NOD, nuclear oligomerization domain protein; $p75^{NTR}$, p75 neurotrophin receptor; PLCγ, phospholipase C γ; qRT-PCR, quantitative RT-PCR; RBC, red blood cell; ROS, reactive oxygen species; SH2, Src homology 2; SHIP1, SH2 domain–containing inositol 5′-phosphatase 1; SFK, Src-family kinase; sRBC, sheep red blood cell; TNF, tumor necrosis factor; TRIM, tripartite motif; XIAP, X-linked inhibitor of apoptosis protein; Bb, *B. burgdorferi*; BSK, Barbour–Stoenner–Kelly.

RIP2-deficient T-cells suffer no apparent defects in proliferation and cytokine secretion upon T-cell receptor ligation (19, 20). Thus, the role of RIP2 in mediating T-cell receptor signaling is still somewhat controversial.

Recognizing a potential Src homology 2 (SH2)-binding motif within RIP2 led us to speculate that RIP2 may be involved in Src-family kinase–mediated signaling pathways. In this work, we describe a specific functional role for RIP2 downstream of Fc γ receptor (FcγR) engagement. We show that RIP2 specifically affects reactive oxygen species (ROS) generation but is dispensable for other functions such as cytokine secretion or phagocytosis. We additionally propose a potential mechanism by which this kinase is activated and discuss implications for IgG-mediated inflammatory diseases and RIP2-targeted therapies.

Results

RIP2 is tyrosine-phosphorylated and activated upon FcγR cross-linking

Identification of the tyrosine autophosphorylation site on RIP2 brought to our attention that, when phosphorylated, this site could serve as a Src-family kinase (SFK) SH2-binding motif, pYE*X*(I/L/P/V) (Fig. 1*A*) (21). With this in mind, we sought to determine the involvement of RIP2 in SFK-mediated signal transduction pathways such as downstream of the FcγR. To determine whether RIP2 could be involved in transducing signals in response to FcγR engagement, we examined whether RIP2 underwent posttranslational modification and/or activation upon FcγR stimulation. We used RAW 264.7 macrophages and WT bone marrow–derived macrophages (BMDMs) and induced FcγR cross-linking using IgG antibodies against BSA + BSA. We then immunoprecipitated RIP2 and assessed tyrosine phosphorylation, a surrogate for RIP2 activity, via Western blotting. Our results show that, for both RAW 264.7 macrophages and WT BMDMs, RIP2 underwent tyrosine phosphorylation (Fig. 1, *B* and *C*) concurrently with activation of other downstream signaling cascades such as NF-κB and MAPK pathways. To ensure that this tyrosine phosphorylation event indicated that RIP2 enzymatic activity was increased, we performed a similar stimulation of the FcγRs, immunoprecipitated RIP2, and performed an *in vitro* kinase (IVK) assay using RIP2 tyrosine autophosphorylation as a readout for enzymatic activity. We found that, indeed, FcγR cross-linking increased RIP2 kinase (Fig. 1, *D* and *E*). We confirmed this further using a second type of IVK assay that measures ADP generated during a kinase reaction. Using this assay, stimulation of RAW 264.7 macrophages and WT BMDMs through the FcγR resulted in a significant increase in enzymatic activity (Fig. 1, *F* and *G*). We also made use of a previously defined panel of genetic RIP2 activation markers (22) and demonstrate that FcγR stimulation of WT BMDMs resulted in a significant up-regulation of all nine genes (Fig. 1*H*). We observed a similar trend, although a reduced effect size, for THP-1 cells differentiated into macrophages and stimulated with human IgG + anti-human IgG (Fig. S1). Altogether, using multiple readouts for measuring RIP2 activity, the data indicate that RIP2 undergoes tyrosine phosphorylation and activation in response to engagement of FcγRs.

RIP2 is involved in signaling downstream of FcγR engagement

To determine the involvement of RIP2 in transducing signals emanating from FcγR engagement, we stimulated WT or RIP2-KO BMDMs with anti-BSA IgG_1 + BSA, anti-BSA IgG_{2a} + BSA, or murine IgG + anti-mIgG and assessed activation of known downstream pathway intermediates via Western blotting. We found that anti-BSA IgG_1 + BSA stimulation (engagement of FcγRIII and FcγRIIB) induces a robust activation of the pathway in WT macrophages but a defect in activation of Syk, PLCγ, and p38 in macrophages lacking RIP2 (Fig. 2*A*). Interestingly, if we stimulated FcγRs by using IgG_{2a} (engagement of FcγRI and FcγRIV) or "bulk" mouse IgG (of all subclasses) these signaling defects are not apparent (Fig. 2, *B* and *C*). These data suggest that RIP2 is involved in transducing signals resulting from FcγR cross-linking specifically when complexes comprise primarily IgG_1 or when FcγRIII/FcγRIIB are preferentially engaged.

RIP2 is not involved in FcγR-mediated cytokine production

Cytokine production is an important downstream effect of FcγR stimulation. To assess whether RIP2 is involved in the FcγR-mediated production of cytokines, we stimulated WT or RIP2-KO BMDMs through their FcγRs for 4 h to isolate RNA for analysis of cytokine expression through qRT-PCR or for 16 h to collect supernatants for analysis of cytokine secretion through ELISA. Although FcγR stimulation induced a significant production of CCL2, CCL3, TNFα, and IL-6 from both genotypes compared with their respective controls when assessed by ELISA (Fig. 3*A*) and a significant increase in the expression of CCL2, CCL3, TNFα, and IL-6 from both genotypes compared with their respective controls when assessed by qRT-PCR (Fig. 3*B*), there was no difference in the responses between WT and RIP2-KO BMDMs upon FcγR stimulation. These data indicate that RIP2 is not involved in FcγR-mediated cytokine production.

RIP2 is not involved in FcγR-mediated phagocytosis

Given that induction of phagocytosis is an important consequence of FcγR engagement, we assessed whether RIP2 instead contributed to the phagocytic capacity of macrophages in response to FcγR stimulation. We stimulated WT or RIP2-KO BMDMs through their FcγRs using PKH26-labeled and antibody-opsonized sheep red blood cells (sRBCs) and measured phagocytosis via flow cytometry and confocal microscopy. Exposure of both WT and RIP2 BMDMs to opsonized sRBCs resulted in a significant increase in the percentage of cells that had phagocytosed opsonized sRBCs compared with unopsonized sRBCs when assessed by flow cytometry (Fig. 4*A*). However, no difference was observed in the number of cells undergoing phagocytosis between WT and RIP2-KO BMDMs. When phagocytosis was assessed by confocal microscopy, a similar trend was observed. Exposure of both WT and RIP2 BMDMs to opsonized sRBCs resulted in a significant increase in the number of particles phagocytosed per macrophage compared with unopsonized controls (Fig. 4*B*). However, no difference was observed in the phagocytic capacity of WT and RIP2-KO BMDMs. These data suggest that RIP2 is not involved in FcγR-mediated phagocytosis.

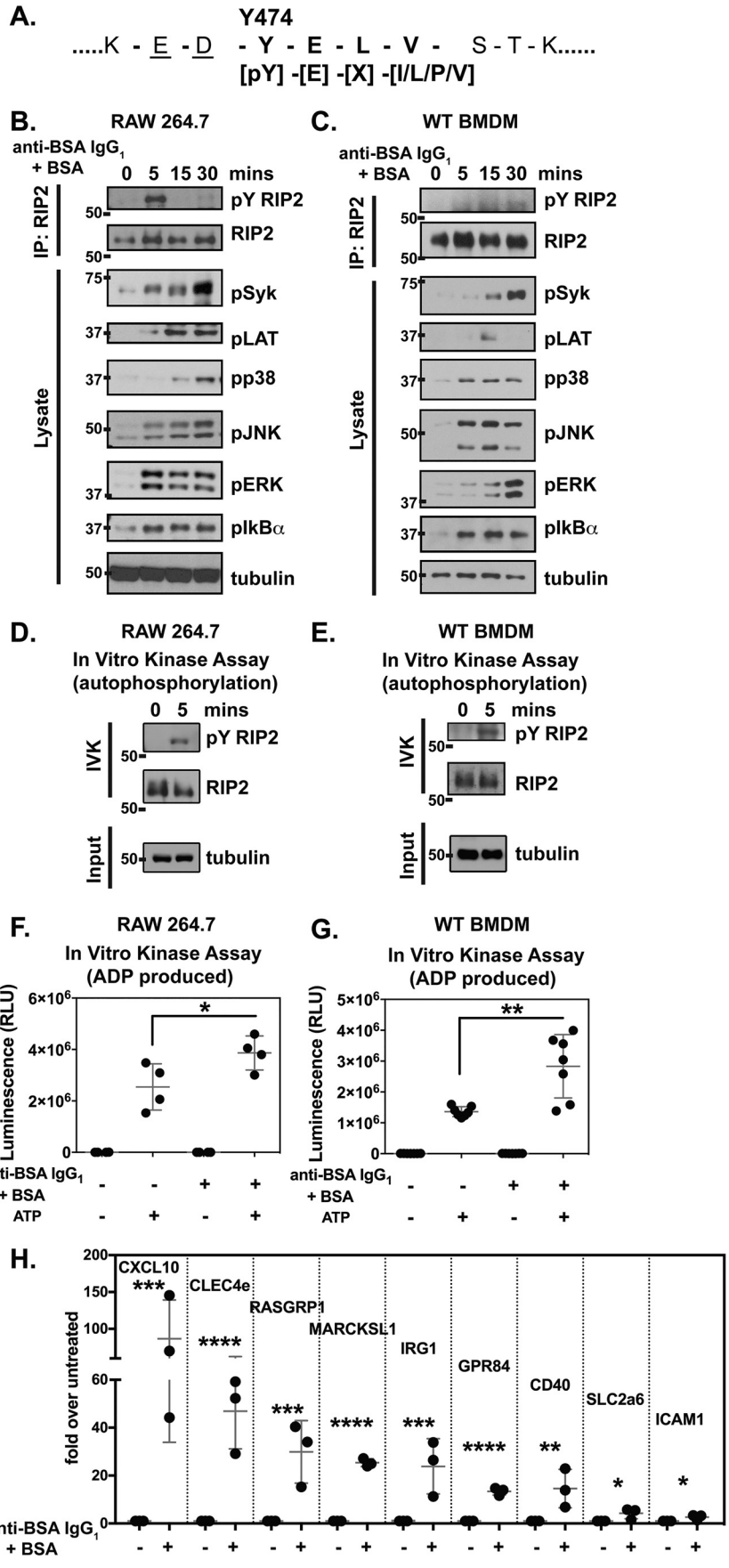
A.
Y474
.....K - E - D - Y - E - L - V - S - T - K.....
[pY] -[E] -[X] -[I/L/P/V]
B.
RAW 264.7
C.
WT BMDM
anti-BSA IgG1
+ BSA
0 5 15 30 mins
IP: RIP2
pY RIP2
RIP2
Lysate
pSyk
pLAT
pp38
pJNK
pERK
plkBα
tubulin
D.
RAW 264.7
In Vitro Kinase Assay
(autophosphorylation)
E.
WT BMDM
IVK
Input
F.
RAW 264.7
In Vitro Kinase Assay
(ADP produced)
G.
WT BMDM
Luminescence (RLU)
ATP
H.
fold over untreated
CXCL10
CLEC4e
RASGRP1
MARCKSL1
IRG1
GPR84
CD40
SLC2a6
ICAM1

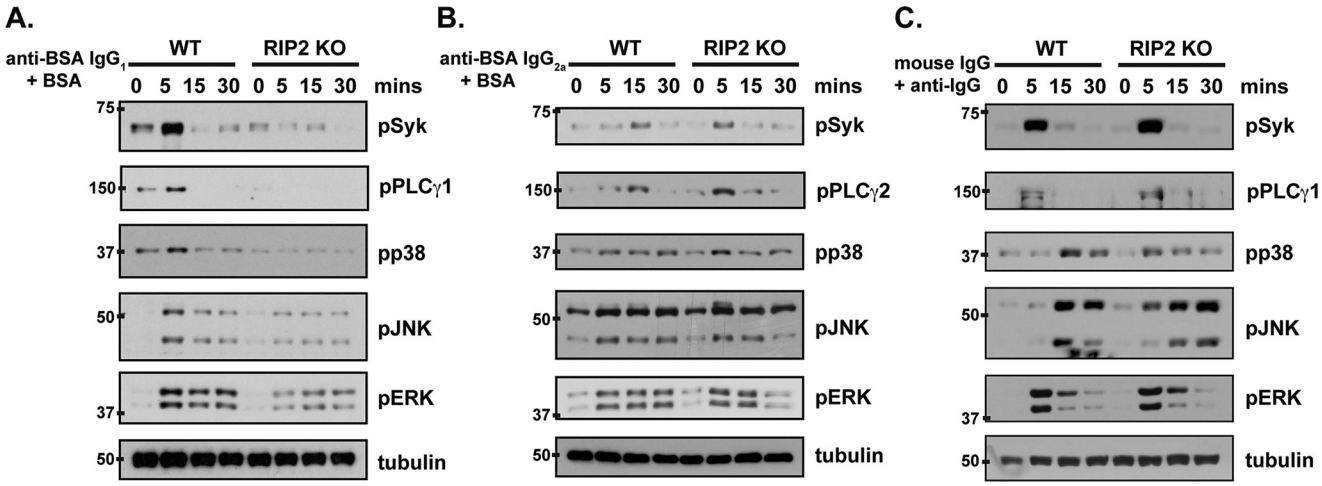

Figure 2. RIP2 is involved in signaling downstream of FcγR engagement. BMDMs from WT and RIP2-KO mice were stimulated with murine anti-BSA IgG_1 + BSA (*A*), murine anti-BSA IgG_{2a} + BSA (*B*), or murine IgG + anti-mIgG (*C*) for the indicated times. Western blotting was performed, and lysates were immunoblotted with the indicated antibodies. Data shown are representative of at least three independent experiments performed.

RIP2 does not affect FcγR-mediated inducible nitric-oxide synthase (iNOS) expression and nitrate/nitrite production

FcγR engagement results not only in phagocytosis of microorganisms and the secretion of proinflammatory mediators but also leads to the production of nitric oxide (NO), a free radical with recognized cytotoxic effects on various microorganisms. To assess whether RIP2 was involved in the generation of NO, we generated BMDMs from WT or RIP2-KO mice, primed these with IFN-γ, and tested the expression of iNOS upon FcγR cross-linking. We tested both protein expression of iNOS via Western blotting (Fig. 5*A*) and gene expression via qRT-PCR (Fig. 5*B*). In both cases, FcγR cross-linking induced iNOS in both genotypes, although it did so to the same extent (Fig. 5, *A* and *B*). Given that NO is rapidly oxidized into nitrite and nitrate, we also quantified the levels of these molecules using a Griess assay (Fig. 5*C*). Again, although FcγR cross-linking induced significant increases in both nitrite and nitrate in both genotypes compared with unstimulated controls, no differences were observed when comparing nitrite/nitrate levels between FcγR-stimulated WT and RIP2-KO BMDMs. These data suggest that RIP2 is not involved in FcγR-mediated iNOS expression or nitrite/nitrate production.

RIP2 is involved in ROS production downstream of FcγR engagement

In phagocytic cells, various immune stimuli, including FcγR engagement, can result in the generation of ROS. Some ROS include superoxide anion, peroxide, hydrogen peroxide, hydroxyl radical, and hydroxyl ions, which mediate antimicrobial activity during the so-called respiratory burst. To assess whether RIP2 is involved in FcγR-mediated ROS production, we generated BMDMs from WT or RIP2-KO mice, primed these with IFN-γ, induced FcγR cross-linking, and assessed ROS production using a ROS-reactive fluorescent probe. In both genotypes, a significant amount of ROS production was observed upon FcγR cross-linking compared with unstimulated cells (Fig. 6, *A* and *B*, represented as percentage of cells stained positive for the probe and as mean fluorescence intensity (MFI) in the FL-1 channel. However, FcγR cross-linking of RIP2-KO BMDMs led to a significantly lower amount of ROS generated when compared with FcγR cross-linking of WT BMDMs (Fig. 6, *A* and *B*). Specificity of the probe for FcγR-induced ROS was verified by using the ROS inhibitor *N*-acetyl-L-cysteine (NAC) in the presence of the Fc cross-linking stimulus and observation of the subsequent loss of fluorescence. These data indicate that RIP2 selectively influences ROS production in response to FcγR engagement.

To determine whether such FcγR-induced ROS production is important in the host response, we also assessed ROS production in WT and RIP2-KO BMDMs in response to unopsonized or opsonized *Borrelia burgdorferi* (Bb), the bacterial agent of Lyme disease. We did observe a similar trend of decreased ROS production in RIP2-KO BMDMs in response to opsonized, but not unopsonized, Bb when compared with the response of WT BMDMs. However, this difference was not

Figure 1. RIP2 is tyrosine-phosphorylated and activated upon FcγR cross-linking. *A*, sequence surrounding the Tyr-474 autophosphorylation site on RIP2, showing that it fulfils the criteria for a Src-family kinase SH2-binding motif. RAW 264.7 macrophages (*B*) and WT BMDMs (*C*) were stimulated with murine anti-BSA IgG_1 + BSA for the indicated times. RIP2 was immunoprecipitated, Western blotting was performed, and IPs were immunoblotted using an anti-phosphotyrosine antibody. Total cell lysates were immunoblotted with the indicated antibodies to assess activation of downstream signaling cascades. IVK assays were performed using RIP2 immunoprecipitated from FcγR-stimulated RAW 264.7 cells (*D*) and WT BMDMs (E) using tyrosine autophosphorylation of RIP2 as a readout of kinase activity. IVK assays were performed using RIP2 immunoprecipitated from FcγR-stimulated RAW 264.7 cells (*F*) and WT BMDMs (*G*) using an ADP-Glo assay. *H*, WT BMDMs were unstimulated or stimulated with murine anti-BSA IgG_1 + BSA for 4 h. RNA was extracted, and qRT-PCR was performed for previously defined genetic RIP2 activation markers. Data in graphs represent means ± S.D. Data are aggregated from at least three independent experiments using $n = 3$–7 mice for the unstimulated condition and $n = 3$–7 mice for the FcγR-stimulated condition. One-way ANOVA with Sidak's multiple comparisons test was used for statistical analysis of IVK assays and a Student's *t* test was used to analyze (log) -fold changes in gene expression (*, $p < 0.05$; **, $p < 0.01$; ***, $p < 0.001$; ****, $p < 0.0001$). *RLU*, relative luciferase units. Longer horizontal lines represent means. *Error bars* represent S.D.

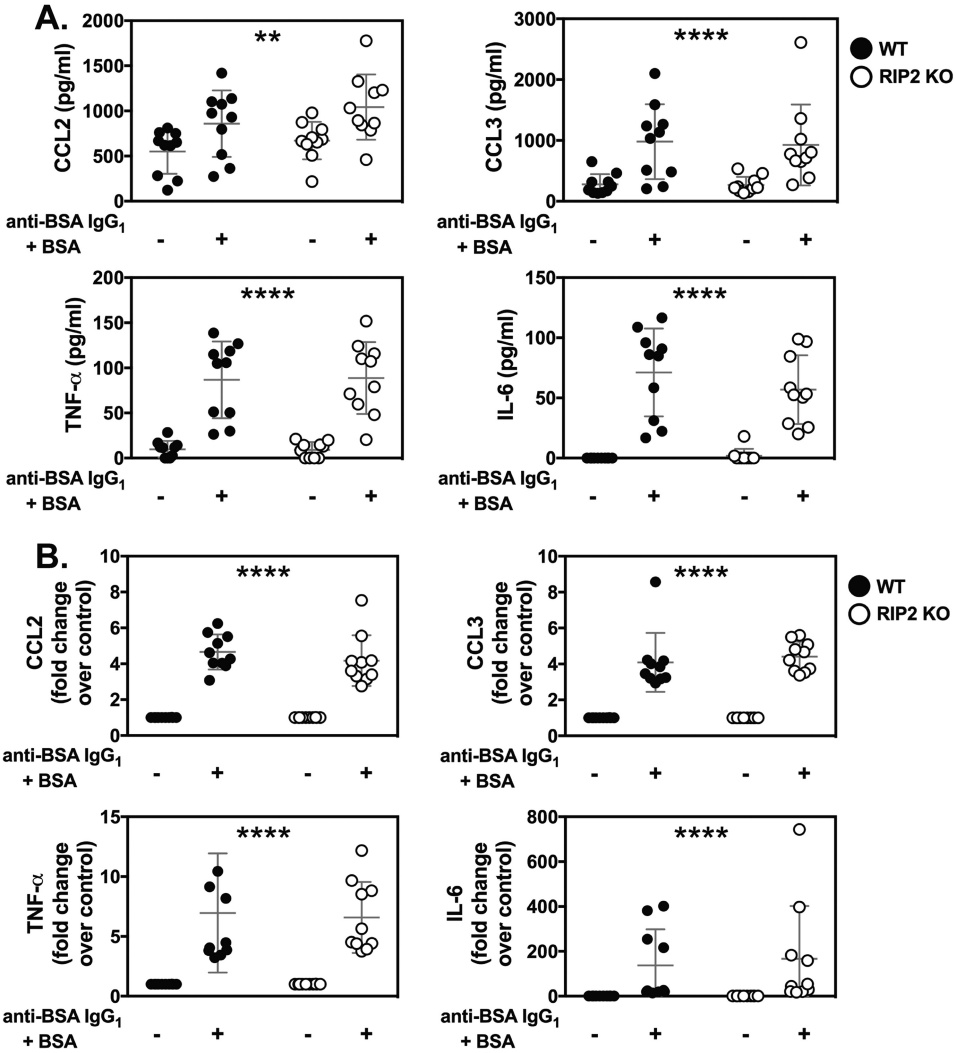

Figure 3. RIP2 is not involved in FcγR-mediated cytokine production. BMDMs from WT and RIP2-KO mice were left unstimulated or were stimulated with murine anti-BSA IgG_1 + BSA for 4 h or for 16 h in low-serum medium. *A*, supernatants were collected after 16 h of stimulation for analysis of cytokine secretion by ELISA. *B*, in a separate set of experiments, RNA was harvested from cells after 4 h to perform qRT-PCR for determining expression of the indicated genes. *Bars* within graphs indicate means ± S.D. Data are aggregated from at least three independent experiments using $n = 10$ mice per group. Two-way ANOVA was used for statistical analysis. For *A* and *B*, no interaction was observed (cytokine secretion and gene up-regulation were similar for WT and RIP2-KO mice upon treatment). Therefore, no further testing was performed. The *p* value for the overall effect of FcγR stimulation is indicated within the graph (**, $p < 0.01$; ****, $p < 0.0001$). Longer horizontal lines represent means. *Error bars* represent S.D.

statistically significant (Fig. S2*A*). We also sought to determine whether such differences may contribute to the intracellular killing of Bb. As depicted in Fig. S2, although we saw clear defects in the ability of RIP2-KO BMDMs to kill unopsonized Bb, opsonization enhanced the killing efficiency of both WT and RIP2-KO BMDMs, so much so that we could not confidently conclude an effect of RIP2 on FcγR-mediated intracellular killing (Fig. S2*B*).

Fgr directly tyrosine-phosphorylates RIP2

One of the first events to occur upon FcγR cross-linking is the phosphorylation of immunoreceptor tyrosine-based activation motifs (ITAMs) by members of the SFKs. Given the potential SFK SH2 interaction motif on RIP2 (Fig. 1*A*), we wanted to determine whether SFKs could mediate RIP2 activation. To assess whether RIP2 may be modified and/or activated by SFKs, we transiently transfected HEK 293T cells with kinase-dead RIP2 in the absence or presence of kinase-live or kinase-dead Fgr or Hck. Upon immunoprecipitation of RIP2, we observed that tyrosine phosphorylation of RIP2 occurred in a manner dependent on the kinase activity of Fgr or Hck (Fig. 7, *A* and *B*). To assess whether these SFKs were directly phosphorylating RIP2, we performed an IVK assay using purified RIP2 or SFKs. These IVK experiments indicated that Fgr, but not Hck, directly mediated tyrosine phosphorylation of RIP2 (Fig. 7, *C* and *D*). Lastly, to determine whether the SFK-mediated phosphorylation influenced the kinase activity of RIP2, we transiently transfected HEK 293T cells with RIP2 in the absence or presence of either Fgr or Hck, immunoprecipitated RIP2, and subjected this to an IVK assay (Fig. 7, *E* and *F*). Using tyrosine autophosphorylation of RIP2 as a readout for kinase activity, these experiments demonstrated that both Fgr and Hck increased the kinase activity of RIP2. Thus, both Fgr and Hck promoted RIP2 tyrosine autophosphorylation and activation. However, only Fgr mediated direct phosphorylation of RIP2.

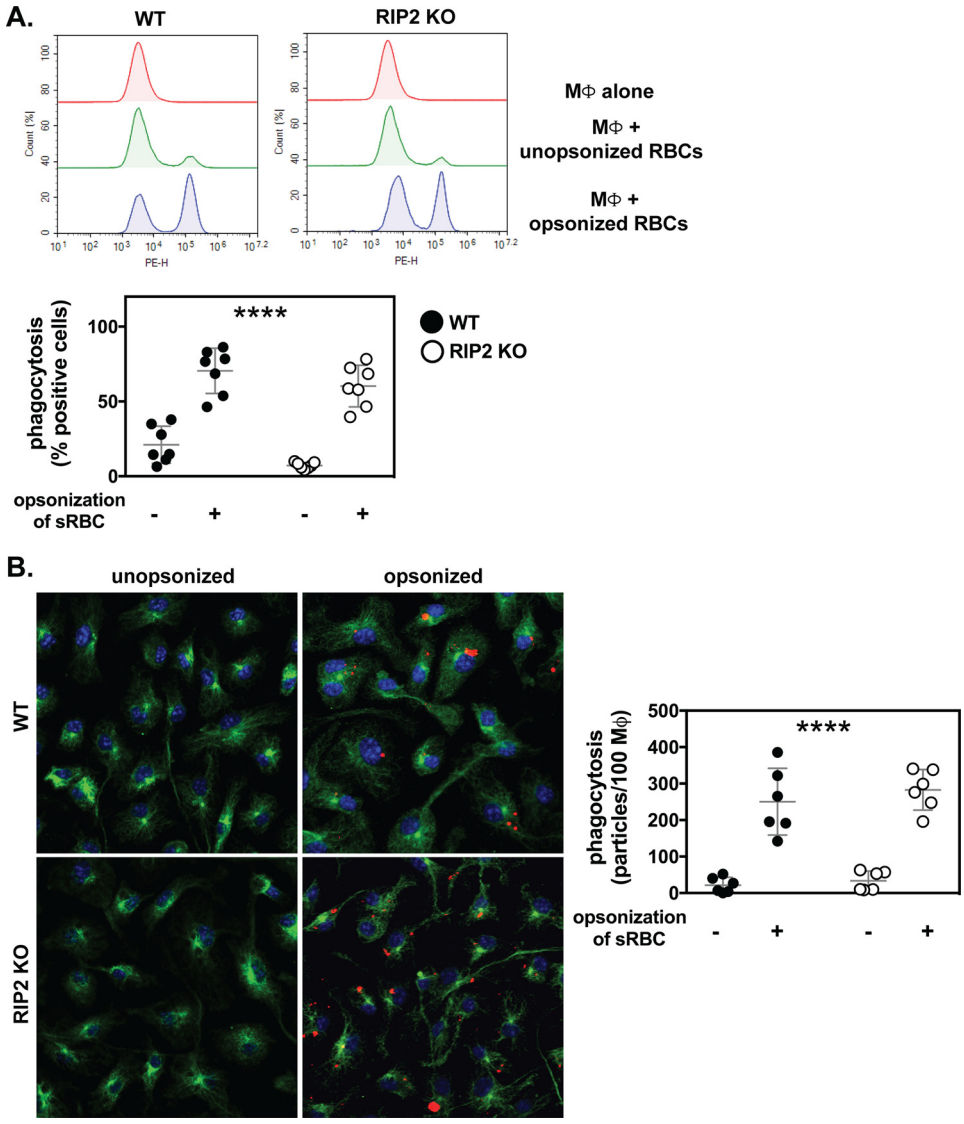

Figure 4. RIP2 is not involved in FcγR-mediated phagocytosis. BMDMs from WT and RIP2-KO mice were incubated with an equal number of PKH26 Red–labeled sRBCs that were previously unopsonized or opsonized with rabbit IgG against sRBCs (1:1600). BMDMs were allowed to phagocytose sRBCs for 30 min at 37 °C. Unphagocytosed sRBCs were osmotically lysed, and BMDMs were washed and analyzed by flow cytometry. *A*, red fluorescence from phagocytosed sRBCs appears as a second peak to the *right* in flow cytometry histograms. Quantitation for flow cytometric analysis of phagocytosis is presented as percentage of cells positive for red fluorescence and is shown *below* the histograms. *B*, phagocytosis of PKH26-labeled opsonized sRBCs by WT and RIP2-KO BMDMs was also analyzed by confocal microscopy. Images of BMDMs incubated with unopsonized or opsonized PKH26-labeled sRBCs were taken after allowing phagocytosis to occur for 30 min. Quantitation for confocal analysis of phagocytosis is presented as particles per 100 macrophages (a total of three 40× fields were counted) shown *beside* the images. *Bars* within graphs represent means ± S.D. Data are aggregated from two independent experiments using $n = 7$ mice per group for flow cytometric analysis of phagocytosis. Data are aggregated from two independent experiments using $n = 6$ mice per group for confocal analysis of phagocytosis. Statistical analysis was performed using a two-way ANOVA. For *A* and *B*, no interaction was observed (phagocytosis of the PKH26-labeled opsonized sRBCs was found to be similar for WT and RIP2-KO mice). Therefore, no further testing was performed. The *p* value for the overall effect of FcγR stimulation is indicated within the graph (****, $p < 0.0001$). *Mϕ*, macrophages. Longer horizontal lines represent means. *Error bars* represent S.D.

NOD2 is required for the observed effects of RIP2 on FcγR-mediated ROS production

To determine whether the ability of RIP2 to promote FcγR-mediated ROS production also required the involvement of the upstream receptor NOD2, we also generated BMDMs from WT and NOD2-KO mice. Similar to RIP2-KO BMDMs, no defects were observed in cytokine production in response to FcγR cross-linking when comparing WT and NOD2-KO BMDMs (Fig. 8, *A* and *B*). As was done previously, we also primed these BMDMs with IFN-γ, induced FcγR cross-linking, and assessed ROS production using a ROS-reactive fluorescent probe. Again, similar to that observed when using RIP2-KO BMDMs, FcγR cross-linking of NOD2-KO BMDMs led to a significantly lower amount of ROS generated when compared with FcγR cross-linking of WT BMDMs (Fig. 8*C*, expressed as either percentage of positive cells or MFI of the ROS-reactive probe). These data suggest that the involvement of RIP2 in FcγR signaling and ROS production depends on NOD2.

Discussion

In this study, we report the functional involvement of RIP2 in FcγR signaling, specifically downstream of FcγRIII/FcγRIIB engagement. We propose that activation of RIP2 occurs very early in this response. In the canonical FcγR-mediated signal-

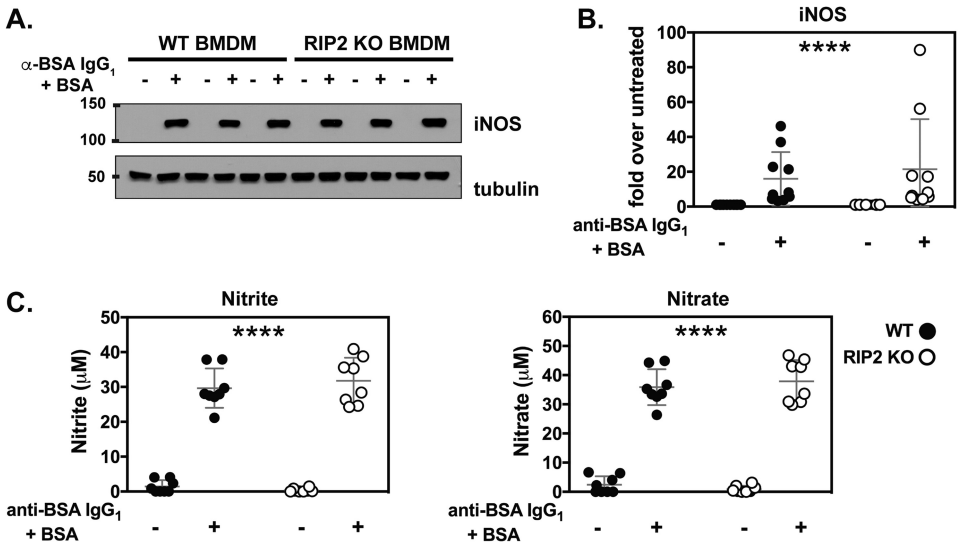

Figure 5. RIP2 does not affect FcγR-mediated iNOS expression and nitrate/nitrite production. *A*, BMDMs from WT and RIP2-KO mice were primed with 100 ng/ml IFN-γ overnight prior to FcγR stimulation for 24 h. Cell lysates were then harvested to perform Western blotting. FcγR-mediated production of iNOS by WT and RIP2-KO BMDMs was assessed by immunoblotting using an anti-iNOS antibody and anti-tubulin antibody as a loading control. Three sets of BMDMs are shown for each genotype. *B*, BMDMs from WT and RIP2-KO mice were left unstimulated or were stimulated with murine anti-BSA IgG_1 + BSA. RNA was harvested from cells after 4 h to perform qRT-PCR to determine expression of iNOS. *C*, IFN-γ–primed WT and RIP2-KO BMDMs were left unstimulated or were stimulated with murine anti-BSA IgG_1 + BSA for 24 h. Cell supernatants were collected for assessment of nitrate/nitrite using a Griess assay. *Bars* within graphs represent means ± S.D. For qRT-PCR analysis of iNOS expression, data are aggregated from two independent experiments using $n = 10$ mice per group. For nitrate/nitrite quantification, data are aggregated from two independent experiments using $n = 8$ mice per group. Statistical analysis was performed using a two-way ANOVA. For *B* and *C*, no interaction was observed (iNOS expression and nitrate/nitrite production as a result of FcγR stimulation were found to be similar for WT and RIP2-KO mice). Therefore, no further testing was performed. The *p* value for the overall effect of FcγR stimulation is indicated within the graph (****, $p < 0.0001$). Longer horizontal lines represent means. *Error bars* represent S.D.

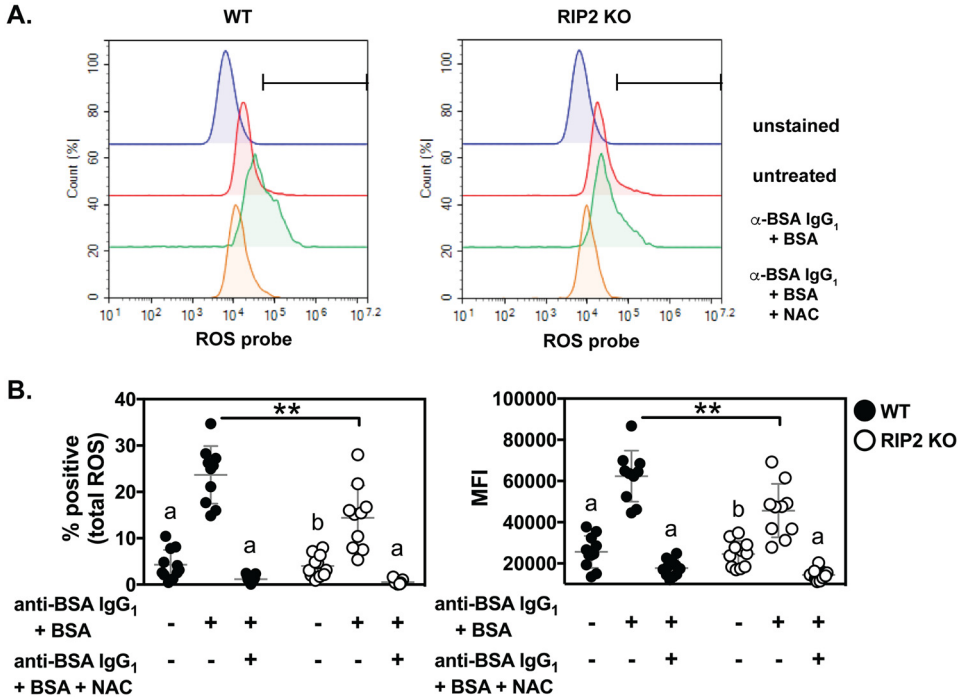

Figure 6. RIP2 is involved in ROS production downstream of FcγR engagement. *A*, BMDMs from WT and RIP2-KO mice were primed with 100 ng/ml IFN-γ overnight prior to FcγR stimulation for 30 min in the presence of 2 μM oxidative stress detection probe. The probe reacts with various ROS to produce a green fluorescent product indicated by increased fluorescence in the FL-1 channel. Treatment of FcγR-stimulated cells with an ROS inhibitor, NAC, results in a leftward shift and a decrease in the FcγR-induced fluorescence. *B*, quantitation for flow cytometric analysis of ROS production is presented as percentage of cells with green fluorescence (compared with unstained control cells) or MFI in the FL-1 channel. *Bars* within graphs represent means ± S.D. Data are aggregated from three experiments using $n = 11$ mice per group. Statistical analysis was performed using a two-way ANOVA with Tukey's multiple comparisons test (**, *b*, $p < 0.01$; *a*, $p < 0.0001$ when compared with the FcγR-stimulated group of the same genotype). Longer horizontal lines represent means. *Error bars* represent S.D.

ing cascade, cross-linking of FcγRs leads to the activation of SFKs such as Fgr and Hck to mediate the phosphorylation of ITAMs on the signal-transducing Fc γ chain to positively influence downstream signaling events. In an as yet undefined mechanism, cross-linking of FcγRs also leads to the activation of NOD2. Both NOD2 and SFKs promote tyrosine phosphory-

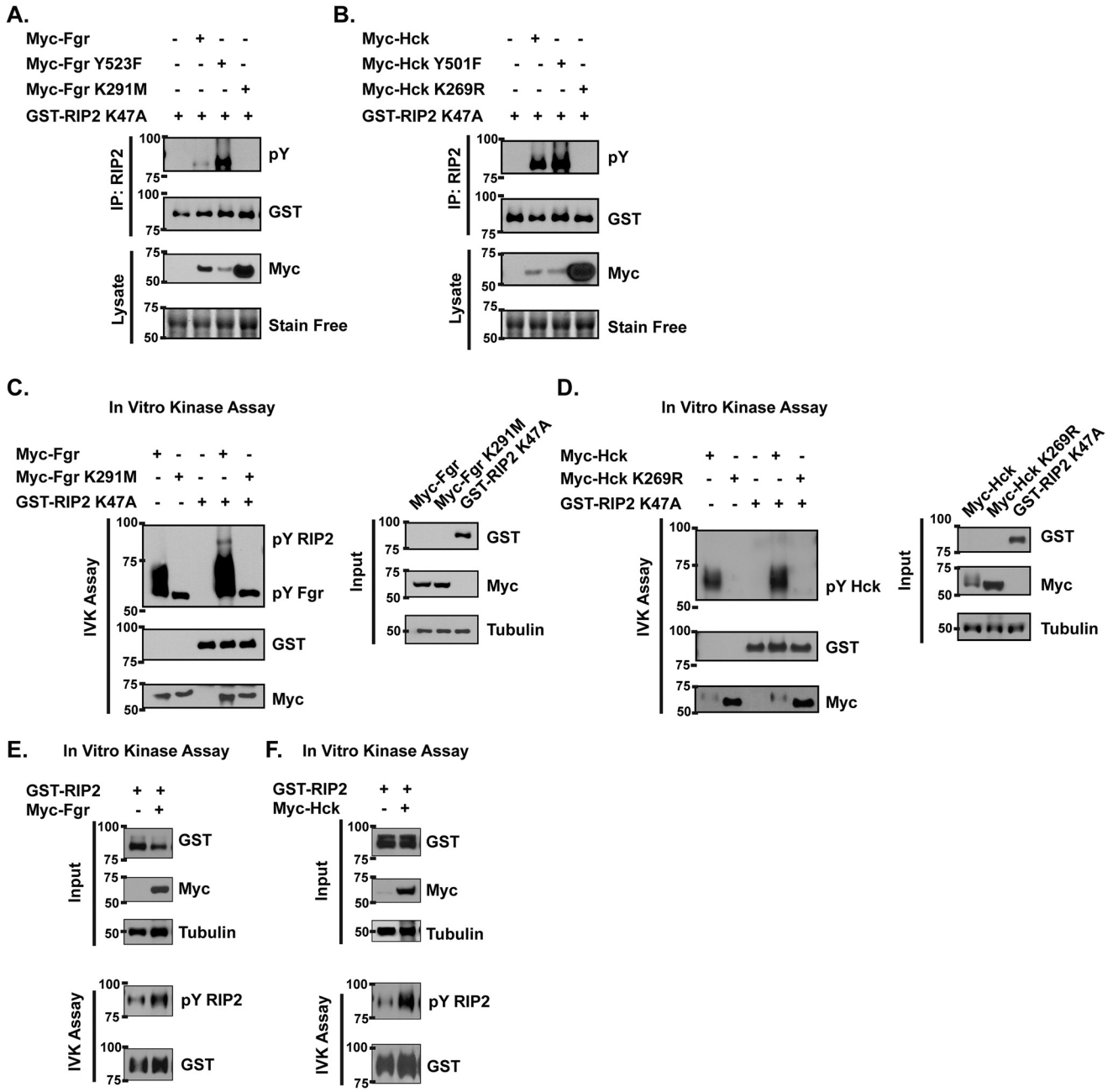

Figure 7. Fgr directly tyrosine-phosphorylates RIP2. HEK293 cells were transiently cotransfected with kinase-dead RIP2 and either WT, constitutively active, or kinase-dead Fgr (*A*) or Hck (*B*). RIP2 was immunoprecipitated, and tyrosine phosphorylation was assessed. HEK293 cells were singly transfected with either kinase-dead RIP2 or with either WT or kinase-dead Fgr (*C*) or Hck (D). RIP2, Fgr, and Hck were immunoprecipitated individually and combined together in an IVK assay as indicated. HEK293 cells were transiently transfected with WT RIP2 with or without Fgr (*E*) or Hck (*F*). RIP2 was immunoprecipitated, and an IVK assay (for tyrosine autophosphorylation) was performed. Data presented are representative of at least three independent experiments performed.

lation and activation of RIP2. This leads to RIP2 selectively influencing FcγRIII/FcγRIIB-induced ROS production but not cytokine secretion, phagocytosis, or nitrate/nitrite production. How it manages to accomplish this is still unclear but is a subject of current investigation.

Although there have been some reports of peptidoglycan-independent mechanisms of activation of NOD1 and NOD2 such as endoplasmic reticulum stress inducers (23), pathogen effector proteins (24), and even viral triggers (25), to our knowledge, this is the first study suggesting that stimulation of FcγRs might somehow cross-talk with NOD2 signaling. So far, no data exist describing a role for NOD2 in binding to immune complexes, in mediating or synergizing with FcγR signaling, or in associating with the various members of the FcγR signaling pathway. IgG_1 complexes, although bound primarily by FcγRIII and FcγRIIB, can also theoretically be detected by FcRn and TRIM21 (26, 27). However, antibody-bound particles do not generally cross plasma membranes unless infectious (*i.e.* antibody-bound viral particles) and can therefore access the cytosolic compartments where TRIM21 resides. Likewise, FcRn only binds IgG under acidic conditions (within endolysosomal compartments of cells or on the cell surface of enterocytes or

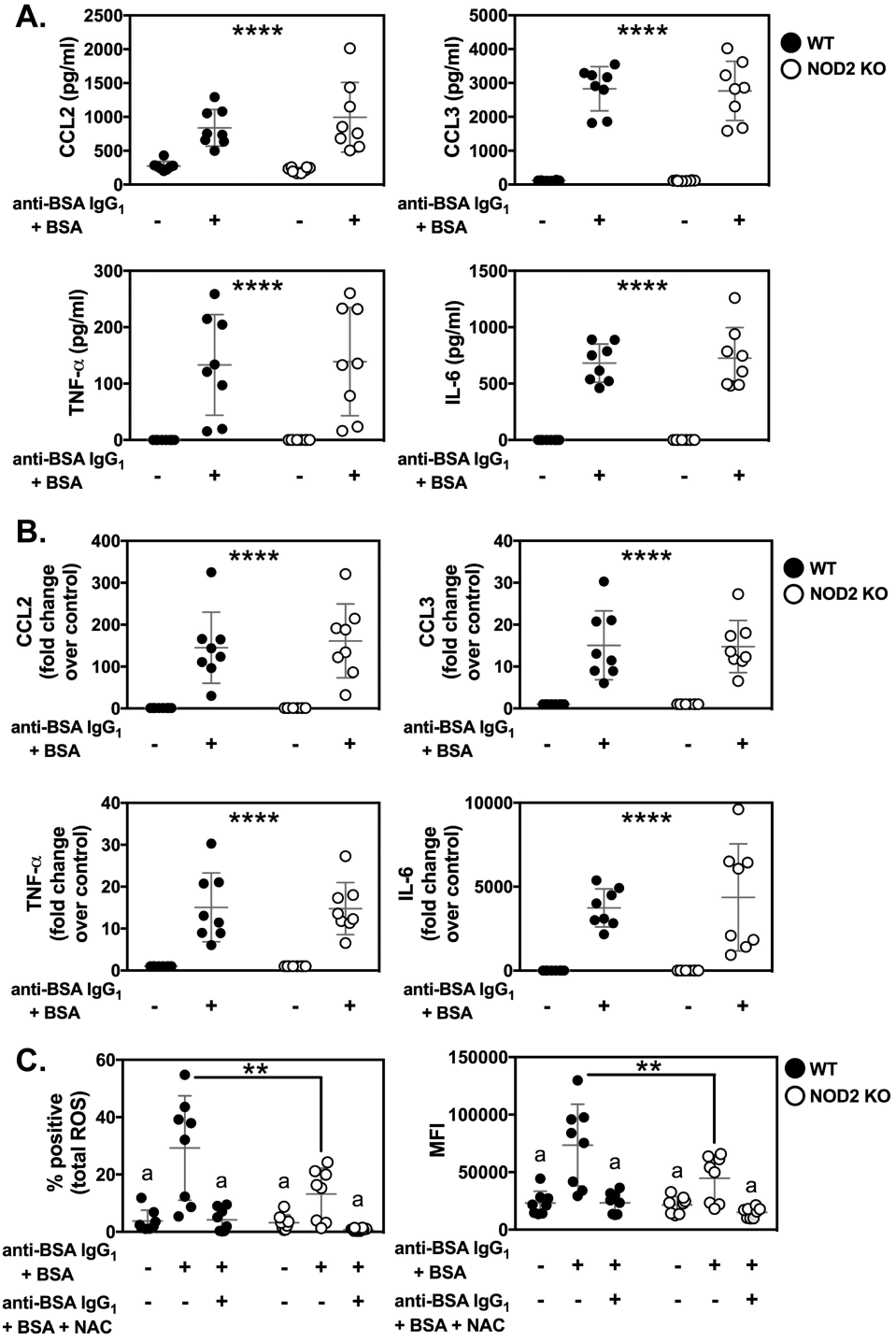

Figure 8. NOD2 is required for the observed effects of RIP2 in FcγR-mediated ROS production. BMDMs from WT and NOD2-KO mice were left unstimulated or were stimulated with murine anti-BSA IgG_1 + BSA for 4 or 16 h in low-serum medium. *A*, supernatants were collected after 16 h of stimulation for analysis of cytokine secretion by ELISA. *B*, in a separate set of experiments, RNA was harvested from cells after 4 h to perform qRT-PCR for determining expression of the indicated genes. *C*, BMDMs from WT and NOD2-KO mice were primed with 100 ng/ml IFN-γ overnight prior to FcγR stimulation for 30 min in the presence of 2 μM oxidative stress detection probe with or without addition of a ROS inhibitor, NAC. Quantitation for flow cytometric analysis of ROS production is presented as percentage of cells with green fluorescence (compared with unstained control cells) or MFI in the FL-1 channel. *Bars* within graphs represent means ± S.D. Data are aggregated from three experiments using $n = 8$ mice per group. Statistical analysis was performed using a two-way ANOVA with Tukey's multiple comparisons test. For *A* and *B*, no interaction was observed (cytokine secretion and gene up-regulation were similar for WT and NOD2-KO mice upon treatment). Therefore, no further testing was performed. The *p* value for the overall effect of FcγR stimulation is indicated within the graph (**, $p < 0.01$; ****, $p < 0.0001$; *a*, $p < 0.0001$ when compared with the FcγR-stimulated group of the same genotype).

other antigen-presenting cells in the acidic gut lumen), leading us to conclude this is not a likely scenario in our system. Furthermore, both FcRn and TRIM21 lack association with an ITAM-bearing γ chain through which SFKs can be recruited and activated. NOD2 has been described to associate with another TRIM family member, TRIM27, which has been dem-

onstrated to promote NOD2 ubiquitination and proteasomal degradation (28). Interaction between NOD2 and TRIM27 was mapped to occur between the TRIM27 PRY-SPRY domain and NOD2 nucleotide-binding domain/NACHT domain. There is ~60% homology at the amino acid level between the PRY-SPRY domains of TRIM21 and TRIM27. Even if NOD2 and TRIM21 were somehow able to associate in the cytosol and these TRIM family members shared a similar function, then engagement would lead instead to down-regulation of the response rather than activation due to the degradation of NOD2. Given this, the exact mechanisms underlying the cross-talk between NOD2 and FcγR signaling still remain to be determined. Furthermore, how RIP2 working downstream of FcγR and NOD2 might synergize or regulate the opposite pathway to influence the immune response would be a worthwhile topic for future study.

A number of outstanding questions still remain. For example, why is there selective participation of RIP2 downstream of some FcγRs but not others? We observed a defect in FcγR signaling when we specifically used immune complexes generated using antibodies of the IgG_1 isotype but not when antibodies of the IgG_{2a} isotype or mixed antibody isotypes were used. It is known that, depending on the isotype, the primary activating Fc receptors can be differentially regulated by the inhibitory Fc receptor FcγRIIB. The higher affinity for FcγRIIB over FcγRIII, in the case of IgG_1, would mean that IgG_1-mediated responses may be more strictly regulated compared with other isotypes (IgG_{2a} or IgG_{2b}) (29). In the classical paradigm of negative regulation mediated by FcγRIIB, receptor cross-linking results in the phosphorylation of immunoreceptor tyrosine-based inhibitory motifs by SFKs, leading to the recruitment of SH2 domain–containing inositol 5′-phosphatase 1 (SHIP1) (for a review, see Ref. 30). SHIP1, in turn, dephosphorylates phosphatidylinositol 3,4,5-trisphosphate, resulting in the generation of phosphatidylinositol 3,4-bisphosphate. This dephosphorylation event not only prevents the recruitment of effector proteins such as Bruton's tyrosine kinase (Btk) and Vav but also promotes the specific recruitment of a different set of effector proteins such as TAPP1/2 and lamellipodin. Whether these regulatory events are affected by the presence and activity of RIP2 is something that remains to be determined. Interestingly, although RIP2 and SHIP1 have not previously been shown to directly interact, SHIP1 has been shown to bind XIAP1, disrupt RIP2–XIAP1 interactions, and regulate NOD2-mediated signaling (31).

Lastly, demonstrating a functional role for RIP2 downstream of the FcγR suggests that manipulation of RIP2 activity (whether that be enzymatic or scaffolding activity) may have wider implications than appreciated previously. Given that dysfunctional FcγR responses have been linked to a number of diseases such as bacterial and viral infections (in concert with complement), vasculitides, systemic lupus erythematosus, rheumatoid arthritis, multiple sclerosis, inflammatory bowel disease, allergic disease, and others, the present work suggests that RIP2 can potentially influence the pathogenesis of these diseases as well. There has been one study that found a significant association between RIP2 SNPs and systemic lupus erythematosus in a Chinese population (32). One SNP resulted in a synonymous change within exon 6 of RIP2, whereas the other occurred within the 3′-UTR of RIP2. Similarly, a RIP2 promoter polymorphism was found to associate with asthma severity in a Japanese population (33). The functional relevance of each of these polymorphisms has, so far, not been tested. Outside of linkage disequilibrium, case-control, and genome-wide association studies, RIP2 has also been implicated in the pathogenesis of multiple sclerosis, inflammatory bowel disease, rheumatoid arthritis, and asthma using genetic knockouts and pharmacological inhibition of RIP2 in animal models of these diseases (22, 34–36). Combined with our findings, this suggests a potential additional mechanism through which loss or inhibition of RIP2 might be conferring therapeutic efficacy. As numerous RIP2-targeted therapies are continually being discovered and developed and one is currently being tested in clinical trials (NCT03358407 and Refs. 37–39), this study broadens their potential use while also shedding light on the possible consequences of RIP2 inhibition in pathways outside of canonical NOD1/2-mediated responses to peptidoglycan.

Experimental procedures

Animals, cells, and antibodies

C57BL/6J (000664), RIP2-KO (007017), and NOD2-KO (005763) mice were purchased from The Jackson Laboratory. Male and female mice between 6 and 10 weeks of age were used for all experimentation. Animals were bred and housed in the Animal Facility at the University of Central Florida Health Science Campus at Lake Nona, an Association for Assessment and Accreditation of Laboratory Animal Care–accredited rodent barrier facility with a strong record of being a specific pathogen-free environment. All animal procedures were performed in accordance with the guidelines of the Institutional Animal Care and Use Committee of the University of Central Florida and using a reviewed and approved animal protocol. The numbers of animals for each strain used per experiment are indicated within the figure legends.

BMDMs were generated by culturing bone marrow for 7 days in DMEM containing 10% heat-inactivated FBS, 1% sodium pyruvate, 1% HEPES, 1% antibiotic-antimycotic, 0.05 mM β-mercaptoethanol, and 25% Ladmac-conditioned medium (Ladmac cells were a gift from Clifford Harding, Case Western Reserve University). Cells were rested in DMEM containing 10% FBS and 1% antibiotic-antimycotic overnight before using in experiments. All media were purchased from Corning, all FBS was from VWR, and supplements were from Invitrogen/Thermo Fisher. Appropriate differentiation of BMDMs was verified by expression of F4/80 and CD11b by flow cytometry.

The RAW 264.7 (TIB-71), THP-1 (TIB-202), and 293T (CRL-3216) cell lines were purchased from ATCC and cultured using the recommended medium and culture conditions. For differentiation of THP-1 cells into macrophages, THP-1 cells were resuspended at a concentration of 1×10^6 cells/ml and plated in 10-cm dishes with 100 ng/ml phorbol 12-myristate 13-acetate. Medium was changed on days 2, 4, and 6 and then used at day 8 for experiments.

Anti-phosphotyrosine (clone P-Tyr-100), anti-phospho-Syk (Tyr-352), anti-phospho-LAT (Tyr-191), anti-phospho-PLCγ1 (clone D6M9S), anti-phospho-PLCγ2 (Tyr-759), anti-phos-

pho-IκBα (clone 5A5), anti-phospho-p44/42 MAPK (ERK1/2) (clone E10), anti-phospho-p38 MAPK (clone 12F8), anti-phospho-JNK (clone 81E11), anti-mouse iNOS, anti-GST tag (clone 91G1), and anti-Myc tag (clone 71D10) were obtained from Cell Signaling Technology. Anti-RIP2 (clone H-300) and anti-tubulin (clone TU-02) were obtained from Santa Cruz Biotechnology. Protein G-agarose was obtained from Invitrogen.

Human and murine FcγR cross-linking

For murine FcγR cross-linking, cells were serum-starved with or without 2.5 μg/ml anti-BSA antibody (IgG_1 clone 9E2C2, Innovative Bioresearch; IgG_{2a} clone BSA-33, Sigma) for 4 h. Afterward, medium was aspirated, and cells were washed once with PBS and then stimulated in low-serum DMEM containing 1 μg/ml BSA for the specific time points indicated. In some experiments, cross-linking was performed using 5 μg/ml murine IgG (Southern Biotechnologies) followed by 10 μg/ml goat anti-mouse IgG (Sigma).

For human FcγR cross-linking, THP-1–derived macrophages were serum-starved for 4 h and then treated with 20 μg/ml human IgG (Sigma) for 30 min on ice. Afterward, cells were washed with PBS, and fresh medium containing 50 μg/ml cross-linking anti-human IgG (Sigma) was added for the time points indicated.

Transfection, immunoprecipitation, and Western blotting

pEBG-RIP2, pEBG-RIP2 K47A, pcDNA3.1 myc-His Hck, pcDNA3.1 myc-His Hck K269R, pcDNA3.1 myc-His Hck Y501F, pcDNA3.1 myc-His Fgr, pcDNA3.1 myc-His Fgr K291M, and pcDNA3.1 myc-His Fgr Y523F were all kind gifts from D. Abbott (Case Western Reserve University). All cDNA constructs used were human. Transient transfection was performed using calcium phosphate transfection of HEK 293T cells. Cells were lysed after 24 h using cell lysis buffer (50 mM Tris (pH 7.5), 150 mM NaCl, 1% Triton X-100, 1 mM EDTA, 1 mM EGTA, 1 mM β-glycerophosphate, 1 mM phenylmethylsulfonyl fluoride, 1 mM $NaVO_4$, 10 nM calyculin A, protease inhibitor mixture (Sigma)). For analysis of RIP2 tyrosine phosphorylation, pervanadate treatment was performed 5 min prior to harvesting the cells. Immunoprecipitation (IP) was carried out by incubating the cleared cell lysates with the respective antibody for 1 h followed by addition of Protein G-Sepharose beads and rotation overnight at 4 °C. IPs were washed at least three times prior to analysis via SDS-PAGE and Western blotting. SDS-PAGE equipment, transfer systems, and nitrocellulose membranes were all from Bio-Rad.

ELISA

Supernatants from stimulated BMDMs were harvested 16 h after FcγR cross-linking for assessing the levels of different cytokines by ELISA. Mouse CCL2, CCL3, IL-6, and TNFα ELISA kits were purchased from eBioscience/Thermo Fisher and used according to the manufacturers' instructions. A Cytation5 plate reader (BioTek) was used for reading absorbance values at 450 nm (with 570-nm background reading subtracted). Cytokine concentrations were calculated by analyzing standard and sample values using a sigmoidal dose-response curve in Prism (GraphPad).

Phagocytosis assay

RBCs (MP Biomedical) were washed twice with PBS and then stained with PKH26 Red Fluorescent Cell Linker kit (Sigma) using a final dye concentration of 3×10^{-6} M to stain 1×10^{8} RBCs/1-ml volume. Cells were stained for 3 min followed by quenching with an equal volume of FBS. The stained cells were washed twice with PBS and subsequently left unopsonized or were opsonized with a 1:1600 dilution of rabbit IgG fraction to sheep RBCs (MP Biomedical) for 1 h at 37 °C. Excess antibody was removed by washing the cell suspension twice with PBS. Erythrocytes were added to macrophages in the 12-well plates in which they were cultured at a ratio of 1:1. Macrophages were incubated on ice prior to addition of the opsonized sRBCs, after which the plates containing macrophages and sRBCs were spun down for 1 min (1000 rpm). The plates were incubated on ice for 10 min. Afterward, PBS was aspirated, warm medium was added, and phagocytosis was allowed to occur at 37 °C for 30 min. Plates were then washed with ice-cold PBS twice followed by hypotonic lysis of any remaining uningested sRBCs. Cells were washed an additional three times with PBS, trypsinized, and then analyzed for phagocytosis by flow cytometry. For flow cytometric analysis of phagocytosis, percent phagocytosis represents the percentage of $PKH26^{+}$ macrophages with the gating determined by signal obtained using macrophages alone.

For analysis of phagocytosis via confocal microscopy, BMDMs were cultured in slide chambers (LabTek) overnight. The same procedure using sRBCs was performed as above. Cells were then fixed with 4% formaldehyde, blocked with blocking buffer (1× PBS, 5% normal serum, 0.3% Triton X-100) for 1 h. Thereafter, cells were incubated overnight with anti-tubulin antibody (Santa Cruz Biotechnology) diluted in antibody dilution buffer 1:100 (1× PBS, 1% BSA, 0.3% Triton X-100). The next day, the cells were washed with 1× Tris-buffered saline, Tween and stained with a 1:1000 dilution of 4′,6-diamidino-2-phenylindole (Sigma) and a 1:1000 dilution of Alexa Fluor 488 anti-mouse antibody (Molecular Probes) in antibody dilution buffer. The slides were analyzed using a Zeiss 710 confocal microscope and associated Zen software. Quantitation for confocal analysis of phagocytosis is presented as particles per 100 macrophages (a total of three 40× fields counted per condition).

Nitrite and total nitrate assay

To measure nitrite and total nitrate production from macrophages, a Greiss reagent kit (Thermo Fisher) was used. BMDMs from WT and RIP2-KO mice were generated and primed with 100 ng/ml IFN-γ overnight. Cells were stimulated via Fc cross-linking as indicated above. After 24 h, cell culture supernatants were collected and assayed using the Greiss reagent kit according to the manufacturer's instructions. Absorbance was measured at 548 nm using a Cytation5 plate reader. The nitrite concentration was calculated based on a nitrite standard curve made in the same culture medium. For total nitrate/nitrite determination, nitrate reductase and enzyme cofactor mixture (obtained from a Nitrate/Nitrite Detection kit from Cayman Chemical) were added to the collected supernatant to convert nitrate to nitrite. The samples were incubated for 1 h at room

temperature to complete the reaction. Total nitrate was then quantified using a Greiss reagent kit with reference to the nitrite standard curve (which was also converted to nitrate). In addition to collecting the supernatant for nitrite/nitrate analysis, cell lysates were also collected for analysis of iNOS expression using Western blotting.

ROS assay

To measure real-time production of ROS from living macrophages, a ROS-ID Total ROS detection kit (Enzo Life Sciences) was used. BMDMs derived from WT and RIP2-KO mice were plated in 6-cm dishes at a concentration of 1×10^6 cells/ml and then primed overnight with 100 ng/ml IFN-γ. The following day, cells were serum-starved in the absence or presence of 2.5 μg/ml IgG_1 anti-BSA. After washing cells with PBS, Fc cross-linking was induced by addition of 1 μg/ml BSA in low-serum, phenol red-free DMEM containing 2 μM oxidative stress detection green dye. Cells were incubated for 30 min at 37 °C and immediately analyzed by flow cytometry. The percentage of FL-1^+ cells was determined with gates set based on unstained cells as a negative control.

Assessment of ROS production in response to opsonized Bb was performed similarly as above with the following modifications. Macrophages were serum-starved for 4 h, scraped off the plates, washed once with PBS, and then left unstimulated or incubated with mock-opsonized or opsonized Bb at a 0.5:1 multiplicity of infection. Incubation of macrophages with Bb was done in low-serum, phenol red-free DMEM containing 2 μM oxidative stress detection green dye. Cells were incubated for 20 min at 37 °C and immediately analyzed by flow cytometry.

RNA extraction and real-time PCR

Macrophages were stimulated for 4 h prior to harvesting the cells for isolation of RNA using an RNeasy kit (Qiagen). RNA extraction was performed according to the manufacturer's instructions. cDNA was synthesized using a Quantitect reverse transcription kit (Qiagen). Real-time PCRs were carried out using iQ SYBR Green Supermix (Bio-Rad) and run on a CFX96 C1000 Real-Time Thermal Cycler (Bio-Rad). The data shown are -fold changes compared with control cells (unstimulated of each genotype) using ΔΔCt analysis. The following primer pairs were used for amplification: mouse CCL2: forward, 5′-CTGCTGTTCACAGTTGCCG-3′; reverse, 5′-GCACAGACCTCTCTCTTGAGC-3′; mouse CCL3: forward, 5′-GAAGGATACAAGCAGCAGCGA-3′; reverse, 5′-GTCTCTTTGGAGTCAGCGCA-3′; mouse TNFα, forward, 5′-GGTGCCTATGTCTCAGCCTC-3′; reverse, 5′-GCTCCTCCACTTGGTGGTTT-3′; mouse IL-6: forward, 5′-CTCTGGGAAATCGTGGAAAT-3′; reverse, 5′-CCAGTTTGGTAGCATCCATC-3′; mouse iNOS: forward, 5′-TTGGTGAAGGGACTGAGCTG-3′; reverse, 5′-TCCAAATCCAACGTTCTCCGT-3′; and mouse glyceraldehyde-3-phosphate dehydrogenase (GAPDH): forward, 5′-TGCCCCCATGTTTGTGATG-3′; reverse, 5′-TGTGGTCATGAGCCCTTCC-3′.

Primers for mouse RIP2 genetic activation markers were used as described previously (22). All primers were synthesized by Integrated DNA Technologies.

IVK assay

To assess enhancement of RIP2's enzymatic activity upon FcγR cross-linking, RAW macrophages, WT BMDMs, or THP-1 macrophages were stimulated through the FcγR for 5 min. RIP2 was immunoprecipitated and subjected to an IVK assay. To assess enhancement of RIP2's enzymatic activity in the presence of Fgr or Hck, RIP2 was transiently transfected into HEK 293T cells with or without Fgr or Hck. RIP2 was immunoprecipitated and subjected to an IVK assay. To assess direct phosphorylation of RIP2 by SFKs, WT or kinase-dead Fgr or Hck and kinase-dead RIP2 were individually transiently transfected into HEK 293T cells. SFKs or RIP2 were immunoprecipitated by their respective tags and combined together in an IVK as indicated. Protein kinase A buffer (25 mM Tris (pH 7.5), 10 mM $MgCl_2$, 5 mM β-glycerophosphate, 2 mM dithiothreitol, 10 mM $MgCl_2$, 0.1 mM Na_3VO_4) was used. IPs were washed thrice in lysis buffer and then thrice in kinase buffer. The reaction was performed in a 40-μl volume using 10 mM ATP (Thermo Fisher). IVK assays were performed for 30 min at 30 °C, after which an equal amount of sample buffer was added, and the entire mixture was boiled for 5 min before analysis of tyrosine phosphorylation by Western blotting.

To assess kinase activity using ADP-Glo (Promega), the IVK reaction was performed in a 25-μl volume using 1 mM Promega Ultrapure ATP. After the assay, ADP-Glo reagent and Kinase-Glo reagent were added and incubated as suggested by the manufacturer. The resulting reactions were then read on a Cytation5 multimode plate reader.

Bb growth conditions and opsonization

The Bb clone used in this study was the-low passage, infectious clone B31 A3-68 Δ*bbe02* (40). Bb cultures were grown at 35 °C in liquid Barbour–Stoenner–Kelly II (BSKII) medium containing gelatin and 6% rabbit serum. For measuring viability, Bb was plated in solid BSK-agarose medium and incubated at 35 °C and 2.5% CO_2.

Fifty-milliliter cultures of Bb in BSKII were grown to mid-log phase, pelleted, and washed twice with HN buffer (50 mM HEPES, 50 mM NaCl (pH 7.5)). The final Bb density was determined using a Petroff–Hauser chamber under darkfield microscopy and adjusted to 10^8/ml using HN buffer. For opsonization, 63 μg of rabbit polyclonal anti-Bb antibody (Abcam) was added to 0.5 ml of the 10^8/ml Bb and incubated at 37 °C for 30 min with end-over-end mixing. Opsonized Bb was collected by centrifugation and washed twice with HN buffer. The opsonized Bb was resuspended in 0.5 ml of HN buffer, and the density was determined using a Petroff–Hauser chamber under darkfield microscopy. Mock opsonization of Bb was performed as above but without the addition of the opsonizing antibody.

Measurement of intracellular killing of Bb by macrophages

BMDMs were serum-starved for 4 h. Prior to the start of the assay, BMDMs were washed once with ice-cold PBS. Ice-cold opsonized or mock-opsonized Bb were added to each well at a multiplicity of infection of 1:1 followed by a brief centrifugation at 4 °C. The supernatant was removed, and the macrophages were washed with ice-cold PBS to remove any unbound Bb.

Prewarmed low-serum DMEM was added to the macrophages, and the cells were incubated at 37 °C with 5% CO_2 for the indicated times to allow for intracellular killing. Macrophages were then washed three times with ice-cold PBS and lysed by addition of 1 ml of distilled H_2O for 4 min. The total lysate was then immediately added to 2 ml of BSKII to halt the lytic effect of distilled H_2O on the released Bb. The number of viable Bb was determined by quantification of the number of cfu in solid BSK medium.

Author contributions—M. G. S. and J. T. T.-A. data curation; M. G. S., O. A. C., G. F. A., M. W. J., and J. T. T.-A. investigation; M. G. S., O. A. C., G. F. A., M. W. J., and J. T. T.-A. methodology; M. G. S. and J. T. T.-A. writing-original draft; M. G. S., O. A. C., G. F. A., M. W. J., and J. T. T.-A. writing-review and editing; G. F. A. and J. T. T.-A. formal analysis; M. W. J. and J. T. T.-A. supervision; M. W. J. and J. T. T.-A. funding acquisition; J. T. T.-A. conceptualization; J. T. T.-A. validation; J. T. T.-A. visualization; O. A. C. and G. F. A. data acquisition.

Acknowledgments—We acknowledge the assistance of Andjie Jeudy and Roopin Singh for genotyping the mice used in this study and for basic laboratory upkeep. We also thank Madelyn Miller for help in editing the draft of the manuscript.

References

1. Inohara, N., del Peso, L., Koseki, T., Chen, S., and Nuñez, G. (1998) RICK, a novel protein kinase containing a caspase recruitment domain, interacts with CLARP and regulates CD95-mediated apoptosis. *J. Biol. Chem.* **273,** 12296–12300 CrossRef Medline
2. Inohara, N., Koseki, T., Lin, J., del Peso, L., Lucas, P. C., Chen, F. F., Ogura, Y., and Nuñez, G. (2000) An induced proximity model for NF-κB activation in the Nod1/RICK and RIP signaling pathways. *J. Biol. Chem.* **275,** 27823–27831 Medline
3. Kobayashi, K., Inohara, N., Hernandez, L. D., Galán, J. E., Nuñez, G., Janeway, C. A., Medzhitov, R., and Flavell, R. A. (2002) RICK/Rip2/CARDIAK mediates signalling for receptors of the innate and adaptive immune systems. *Nature* **416,** 194–199 CrossRef Medline
4. McCarthy, J. V., Ni, J., and Dixit, V. M. (1998) RIP2 is a novel NF-κB-activating and cell death-inducing kinase. *J. Biol. Chem.* **273,** 16968–16975 CrossRef Medline
5. Park, J. H., Kim, Y. G., McDonald, C., Kanneganti, T. D., Hasegawa, M., Body-Malapel, M., Inohara, N., and Nuñez, G. (2007) RICK/RIP2 mediates innate immune responses induced through Nod1 and Nod2 but not TLRs. *J. Immunol.* **178,** 2380–2386 CrossRef Medline
6. Thome, M., Hofmann, K., Burns, K., Martinon, F., Bodmer, J. L., Mattmann, C., and Tschopp, J. (1998) Identification of CARDIAK, a RIP-like kinase that associates with caspase-1. *Curr. Biol.* **8,** 885–888 CrossRef Medline
7. Tigno-Aranjuez, J. T., Asara, J. M., and Abbott, D. W. (2010) Inhibition of RIP2's tyrosine kinase activity limits NOD2-driven cytokine responses. *Genes Dev.* **24,** 2666–2677 CrossRef Medline
8. Chamaillard, M., Hashimoto, M., Horie, Y., Masumoto, J., Qiu, S., Saab, L., Ogura, Y., Kawasaki, A., Fukase, K., Kusumoto, S., Valvano, M. A., Foster, S. J., Mak, T. W., Nuñez, G., and Inohara, N. (2003) An essential role for NOD1 in host recognition of bacterial peptidoglycan containing diaminopimelic acid. *Nat. Immunol.* **4,** 702–707 CrossRef Medline
9. Girardin, S. E., Boneca, I. G., Carneiro, L. A., Antignac, A., Jéhanno, M., Viala, J., Tedin, K., Taha, M. K., Labigne, A., Zähringer, U., Coyle, A. J., DiStefano, P. S., Bertin, J., Sansonetti, P. J., and Philpott, D. J. (2003) Nod1 detects a unique muropeptide from Gram-negative bacterial peptidoglycan. *Science* **300,** 1584–1587 CrossRef Medline
10. Inohara, N., Ogura, Y., Fontalba, A., Gutierrez, O., Pons, F., Crespo, J., Fukase, K., Inamura, S., Kusumoto, S., Hashimoto, M., Foster, S. J., Moran, A. P., Fernandez-Luna, J. L., and Nuñez, G. (2003) Host recognition of bacterial muramyl dipeptide mediated through NOD2. Implications for Crohn's disease. *J. Biol. Chem.* **278,** 5509–5512 CrossRef Medline
11. Divangahi, M., Mostowy, S., Coulombe, F., Kozak, R., Guillot, L., Veyrier, F., Kobayashi, K. S., Flavell, R. A., Gros, P., and Behr, M. A. (2008) NOD2-deficient mice have impaired resistance to *Mycobacterium tuberculosis* infection through defective innate and adaptive immunity. *J. Immunol.* **181,** 7157–7165 CrossRef Medline
12. Frutuoso, M. S., Hori, J. I., Pereira, M. S., Junior, D. S., Sônego, F., Kobayashi, K. S., Flavell, R. A., Cunha, F. Q., and Zamboni, D. S. (2010) The pattern recognition receptors Nod1 and Nod2 account for neutrophil recruitment to the lungs of mice infected with *Legionella pneumophila*. *Microbes Infect.* **12,** 819–827 CrossRef Medline
13. Geddes, K., Rubino, S., Streutker, C., Cho, J. H., Magalhaes, J. G., Le Bourhis, L., Selvanantham, T., Girardin, S. E., and Philpott, D. J. (2010) Nod1 and Nod2 regulation of inflammation in the *Salmonella* colitis model. *Infect. Immun.* **78,** 5107–5115 CrossRef Medline
14. Shimada, K., Chen, S., Dempsey, P. W., Sorrentino, R., Alsabeh, R., Slepenkin, A. V., Peterson, E., Doherty, T. M., Underhill, D., Crother, T. R., and Arditi, M. (2009) The NOD/RIP2 pathway is essential for host defenses against *Chlamydophila pneumoniae* lung infection. *PLoS Pathog.* **5,** e1000379 CrossRef Medline
15. Uhlén, M., Fagerberg, L., Hallström, B. M., Lindskog, C., Oksvold, P., Mardinoglu, A., Sivertsson, Å., Kampf, C., Sjöstedt, E., Asplund, A., Olsson, I., Edlund, K., Lundberg, E., Navani, S., Szigyarto, C. A., *et al.* (2015) Proteomics. Tissue-based map of the human proteome. *Science* **347,** 1260419 CrossRef Medline
16. Kisiswa, L., Fernández-Suárez, D., Sergaki, M. C., and Ibáñez, C. F. (2018) RIP2 gates TRAF6 interaction with death receptor p75(NTR) to regulate cerebellar granule neuron survival. *Cell Rep.* **24,** 1013–1024 CrossRef Medline
17. Shimada, K., Porritt, R. A., Markman, J. L., O'Rourke, J. G., Wakita, D., Noval Rivas, M., Ogawa, C., Kozhaya, L., Martins, G. A., Unutmaz, D., Baloh, R. H., Crother, T. R., Chen, S., and Arditi, M. (2018) T-cell-intrinsic receptor interacting protein 2 regulates pathogenic T helper 17 cell differentiation. *Immunity* **49,** 873–885.e7 CrossRef Medline
18. Ruefli-Brasse, A. A., French, D. M., and Dixit, V. M. (2003) Regulation of NF-κB-dependent lymphocyte activation and development by paracaspase. *Science* **302,** 1581–1584 CrossRef Medline
19. Hall, H. T., Wilhelm, M. T., Saibil, S. D., Mak, T. W., Flavell, R. A., and Ohashi, P. S. (2008) RIP2 contributes to Nod signaling but is not essential for T cell proliferation, T helper differentiation or TLR responses. *Eur. J. Immunol.* **38,** 64–72 CrossRef Medline
20. Nembrini, C., Reissmann, R., Kopf, M., and Marsland, B. J. (2008) Effective T-cell immune responses in the absence of the serine/threonine kinase RIP2. *Microbes Infect.* **10,** 522–530 CrossRef Medline
21. Liu, B. A., Jablonowski, K., Shah, E. E., Engelmann, B. W., Jones, R. B., and Nash, P. D. (2010) SH2 domains recognize contextual peptide sequence information to determine selectivity. *Mol. Cell. Proteomics* **9,** 2391–2404 CrossRef Medline
22. Tigno-Aranjuez, J. T., Benderitter, P., Rombouts, F., Deroose, F., Bai, X., Mattioli, B., Cominelli, F., Pizarro, T. T., Hoflack, J., and Abbott, D. W. (2014) *In vivo* inhibition of RIPK2 kinase alleviates inflammatory disease. *J. Biol. Chem.* **289,** 29651–29664 CrossRef Medline
23. Keestra-Gounder, A. M., Byndloss, M. X., Seyffert, N., Young, B. M., Chávez-Arroyo, A., Tsai, A. Y., Cevallos, S. A., Winter, M. G., Pham, O. H., Tiffany, C. R., de Jong, M. F., Kerrinnes, T., Ravindran, R., Luciw, P. A., McSorley, S. J., *et al.* (2016) NOD1 and NOD2 signalling links ER stress with inflammation. *Nature* **532,** 394–397 CrossRef Medline
24. Meinzer, U., Barreau, F., Esmiol-Welterlin, S., Jung, C., Villard, C., Léger, T., Ben-Mkaddem, S., Berrebi, D., Dussaillant, M., Alnabhani, Z., Roy, M., Bonacorsi, S., Wolf-Watz, H., Perroy, J., Ollendorff, V., *et al.* (2012) *Yersinia pseudotuberculosis* effector YopJ subverts the Nod2/RICK/TAK1 pathway and activates caspase-1 to induce intestinal barrier dysfunction. *Cell Host Microbe* **11,** 337–351 CrossRef Medline
25. Sabbah, A., Chang, T. H., Harnack, R., Frohlich, V., Tominaga, K., Dube, P. H., Xiang, Y., and Bose, S. (2009) Activation of innate immune antiviral responses by Nod2. *Nat. Immunol.* **10,** 1073–1080 CrossRef Medline

26. Simister, N. E., and Mostov, K. E. (1989) An Fc receptor structurally related to MHC class I antigens. *Nature* **337,** 184–187 CrossRef Medline
27. Rhodes, D. A., and Trowsdale, J. (2007) TRIM21 is a trimeric protein that binds IgG Fc via the B30.2 domain. *Mol. Immunol.* **44,** 2406–2414 CrossRef Medline
28. Zurek, B., Schoultz, I., Neerincx, A., Napolitano, L. M., Birkner, K., Bennek, E., Sellge, G., Lerm, M., Meroni, G., Söderholm, J. D., and Kufer, T. A. (2012) TRIM27 negatively regulates NOD2 by ubiquitination and proteasomal degradation. *PLoS One* **7,** e41255 CrossRef Medline
29. Nimmerjahn, F., and Ravetch, J. V. (2006) Fcγ receptors: old friends and new family members. *Immunity* **24,** 19–28 CrossRef Medline
30. Pauls, S. D., and Marshall, A. J. (2017) Regulation of immune cell signaling by SHIP1: a phosphatase, scaffold protein, and potential therapeutic target. *Eur. J. Immunol.* **47,** 932–945 CrossRef Medline
31. Condé, C., Rambout, X., Lebrun, M., Lecat, A., Di Valentin, E., Dequiedt, F., Piette, J., Gloire, G., and Legrand, S. (2012) The inositol phosphatase SHIP-1 inhibits NOD2-induced NF-κB activation by disturbing the interaction of XIAP with RIP2. *PLoS One* **7,** e41005 CrossRef Medline
32. Li, J., Tian, J., Ma, Y., Cen, H., Leng, R. X., Lu, M. M., Chen, G. M., Feng, C. C., Tao, J. H., Pan, H. F., and Ye, D. Q. (2012) Association of RIP2 gene polymorphisms and systemic lupus erythematosus in a Chinese population. *Mutagenesis* **27,** 319–322 CrossRef Medline
33. Nakashima, K., Hirota, T., Suzuki, Y., Akahoshi, M., Shimizu, M., Jodo, A., Doi, S., Fujita, K., Ebisawa, M., Yoshihara, S., Enomoto, T., Shirakawa, T., Kishi, F., Nakamura, Y., and Tamari, M. (2006) Association of the RIP2 gene with childhood atopic asthma. *Allergol. Int.* **55,** 77–83 CrossRef Medline
34. Vieira, S. M., Cunha, T. M., França, R. F., Pinto, L. G., Talbot, J., Turato, W. M., Lemos, H. P., Lima, J. B., Verri, W. A., Jr., Almeida, S. C., Ferreira, S. H., Louzada-Junior, P., Zamboni, D. S., and Cunha, F. Q. (2012) Joint NOD2/RIPK2 signaling regulates IL-17 axis and contributes to the development of experimental arthritis. *J. Immunol.* **188,** 5116–5122 CrossRef Medline
35. Nachbur, U., Stafford, C. A., Bankovacki, A., Zhan, Y., Lindqvist, L. M., Fiil, B. K., Khakham, Y., Ko, H. J., Sandow, J. J., Falk, H., Holien, J. K., Chau, D., Hildebrand, J., Vince, J. E., Sharp, P. P., *et al.* (2015) A RIPK2 inhibitor delays NOD signalling events yet prevents inflammatory cytokine production. *Nat. Commun.* **6,** 6442 CrossRef Medline
36. Miller, M. H., Shehat, M. G., Alcedo, K. P., Spinel, L. P., Soulakova, J., and Tigno-Aranjuez, J. T. (2018) Frontline science: RIP2 promotes house dust mite-induced allergic airway inflammation. *J. Leukoc. Biol.* **104,** 447–459 CrossRef Medline
37. Goncharov, T., Hedayati, S., Mulvihill, M. M., Izrael-Tomasevic, A., Zobel, K., Jeet, S., Fedorova, A. V., Eidenschenk, C., deVoss, J., Yu, K., Shaw, A. S., Kirkpatrick, D. S., Fairbrother, W. J., Deshayes, K., and Vucic, D. (2018) Disruption of XIAP-RIP2 association blocks NOD2-mediated inflammatory signaling. *Mol. Cell* **69,** 551–565.e7 CrossRef Medline
38. Haile, P. A., Votta, B. J., Marquis, R. W., Bury, M. J., Mehlmann, J. F., Singhaus, R., Jr., Charnley, A. K., Lakdawala, A. S., Convery, M. A., Lipshutz, D. B., Desai, B. M., Swift, B., Capriotti, C. A., Berger, S. B., Mahajan, M. K., *et al.* (2016) The identification and pharmacological characterization of 6-(tert-butylsulfonyl)-N-(5-fluoro-1H-indazol-3-yl)quinolin-4-amine (GSK583), a highly potent and selective inhibitor of RIP2 Kinase. *J. Med. Chem.* **59,** 4867–4880 CrossRef Medline
39. Salla, M., Aguayo-Ortiz, R., Danmaliki, G. I., Zare, A., Said, A., Moore, J., Pandya, V., Manaloor, R., Fong, S., Blankstein, A. R., Gibson, S. B., Garcia, L. R., Meier, P., Bhullar, K. S., Hubbard, B. P., *et al.* (2018) Identification and characterization of novel receptor-interacting serine/threonine-protein kinase 2 inhibitors using structural similarity analysis. *J. Pharmacol. Exp. Ther.* **365,** 354–367 CrossRef Medline
40. Rego, R. O., Bestor, A., and Rosa, P. A. (2011) Defining the plasmid-borne restriction-modification systems of the Lyme disease spirochete *Borrelia burgdorferi*. *J. Bacteriol.* **193,** 1161–1171 CrossRef Medline